

Quantitative Assessment of Asymmetric Choroidal Outflow in Pachychoroid Eyes on Ultra-Widefield Indocyanine Green Angiography

Jesse J. Jung,^{1,2} Daryle Jason G. Yu,³ Kazuyo Ito,³ Soraya Rofagha,¹ Scott S. Lee,¹ and Quan V. Hoang^{3,4}

¹East Bay Retina Consultants, Oakland, California, United States

²Department of Ophthalmology, University of California, San Francisco, California, United States

³Singapore Eye Research Institute, Singapore National Eye Centre, Duke-NUS, Singapore

⁴Department of Ophthalmology, Columbia University Vagelos College of Physicians and Surgeons, New York, New York, United States

Correspondence: Jesse J. Jung, East Bay Retina Consultants, 3300 Telegraph Avenue, Oakland, CA 94609, USA; jung.jesse@gmail.com.

Received: May 19, 2020

Accepted: June 20, 2020

Published: July 31, 2020

Citation: Jung JJ, Yu DJG, Ito K, Rofagha S, Lee SS, Hoang QV. Quantitative assessment of asymmetric choroidal outflow in pachychoroid eyes on ultra-widefield indocyanine green angiography. *Invest Ophthalmol Vis Sci.* 2020;61(8):50. <https://doi.org/10.1167/iovs.61.8.50>

PURPOSE. To quantitatively demonstrate asymmetric choroidal outflow in pachychoroid (central serous chorioretinopathy [CSC]/pachychoroid pigment epitheliopathy [PPE]) eyes using mid-phase, ultra-widefield indocyanine green angiography (UWF ICGA) images.

METHODS. Eyes with a clinical diagnosis of CSC/PPE were imaged with multimodal imaging including UWF ICGA (Optos California). Quadrant brightness was measured by manually segmenting based on vortex vein location, calculating the brightness “max-min” value to assess nonuniformity between quadrants, and comparing between CSC/PPE and control eyes. A multivariate linear regression was performed to determine, across individual eyes, which specific quadrants have the greatest brightness in pachychoroid eyes, after taking into account patient-eye-specific variability.

RESULTS. Thirty-three eyes (18 patients) with CSC/PPE along with 16 eyes of 9 controls had a mean age of 51.94 ± 9.72 vs. 53.78 ± 17.92 years ($P = 0.731$), respectively. Max-min analysis showed significantly increased likelihood of nonuniform drainage between vortex veins in both CSC/PPE and control eyes. Multivariate linear regression in control eyes showed that on average, the inferotemporal quadrant was significantly brighter than the superonasal quadrant (9.72 units, $P < 0.001$). Among CSC/PPE eyes, adjusting for the preferential, nonuniform drainage in control eyes, the inferonasal and inferotemporal quadrants in CSC/PPE eyes remained significantly brighter than the reference quadrant by 5.36 units ($P = 0.034$) and 7.51 units ($P = 0.008$), respectively.

CONCLUSIONS. Asymmetric choroidal venous outflow occurs in both control and CSC/PPE eyes based on UWF ICGA quantitative brightness levels in each quadrant. Increased brightness levels along inferior quadrants in mid-phase ICGA images suggest venous outflow congestion among eyes with CSC or PPE.

Keywords: angiography, central serous chorioretinopathy, choroidal outflow, indocyanine green angiography, pachychoroid, vortex veins, ultra-widefield imaging

Central serous chorioretinopathy (CSC) is the fourth most common cause of nonsurgical maculopathy after age-related macular degeneration, diabetic retinopathy, and branch retinal vein occlusion.¹ This disease is characterized by sudden blurring or dimming of vision, micropsia, metamorphopsia, paracentral scotoma, or decrease in color vision.¹ CSC occurs frequently in otherwise healthy, young, or middle-aged patients who are predominantly male and develop exudative detachment of the neurosensory retina, often associated with an underlying focal or multifocal serous elevation of the retinal pigment epithelium (RPE).^{2,3} Other associated risk factors include exogenous steroid use, type A personality, and endogenous hypercortisol conditions.^{4,5}

RPE changes overlying areas of choroidal thickening have been observed in fellow eyes of patients with unilateral CSC, described as pachychoroid pigment epitheliopathy (PPE).² PPE was previously considered a type of forme fruste of CSC, as it is usually asymptomatic and the majority of the eyes do not develop frank neurosensory retinal detachments.² Clinically, reduced fundus tessellation, absence of drusen, mottling of the RPE, and irregular areas of RPE elevation are frequently observed.² Thickened choroid and dilated Haller's layer vessels on enhanced-depth imaging optical coherence tomography (EDI-OCT) were observed in both conditions.^{2,6,7} With similar underlying choroidal findings, CSC and PPE share a common pathophysiologic mechanism, suggesting both should be considered part of a disease

spectrum known as pachychoroid disease.⁸ This spectrum includes CSC, PPE, pachychoroid neovasculopathy (PNV), polypoidal choroidal vasculopathy (PCV)/aneurysmal type 1 neovascularization, focal choroidal excavation, and peripapillary pachychoroid syndrome.^{2,8-13} Shared features include the characteristic attenuation of the choriocapillaris overlying dilated choroidal veins leading to progressive dysfunction of the RPE and risk of choroidal neovascularization.¹³ Furthermore, history of CSC is considered a risk for the development of PCV.¹⁴⁻¹⁷

Focal RPE dysfunction was originally thought to be the main pathology for CSC, but Negi and Marmor^{18,19} demonstrated that a simple barrier defect in the RPE alone did not lead to neurosensory retinal detachment in experimental studies. RPE dysfunction has been found to correspond to areas of increased choroidal hyperpermeability on late-phase indocyanine green angiography (ICGA) images^{20,21} thought to be secondary to hydrostatic dysfunction of the choroid^{14,20,22-28} and areas of increased choroidal thickness²⁹ observed with cross-sectional EDI-OCT images attributed to luminal dilatation mainly in the outer vascular layer of the choroid.^{6,7,30,31} These choroidal abnormalities then lead to the development of an overlying serous pigment epithelial detachment (PED) and subsequent detachment of the neurosensory retina in the macular region.³²⁻³⁴

However, these previous ICGA studies were limited to the posterior pole without extensive peripheral imaging of the vortex veins. Ultra-widefield imaging (UWF) has expanded our ability to capture the peripheral retina up to 200 degrees with ICGA.³⁵⁻⁴⁰ Previous qualitative studies of UWF ICGA hypothesized that in CSC eyes, there may be a congestive component with decreased outflow through the peripheral vortex veins,^{38,41,42} and one study of UWF ICGA using densitometry analysis of the entire choroidal vasculature demonstrated increased choroidal vessel density in CSC versus normal eyes but did not evaluate PPE eyes or compare the flow signal in separate quadrants based on the location of the vortex veins. In this study, we quantitatively evaluated the brightness signal of the mid-phase UWF ICGA as a surrogate for vascular outflow congestion in CSC and PPE eyes compared to age-matched, nonpachychoroid control eyes and traced the entire course of the choroidal outflow up to the ampulla of each respective vortex vein in a single image acquisition.

METHODS

This retrospective, cross-sectional comparative cohort study design (protocol #20160664) was approved by the Western Institutional Review Board (Puyallup, WA). This study complied with the Health Insurance Portability and Accountability Act of 1996 and followed the tenets of the Declaration of Helsinki.

Participants

Patients with characteristics of treatment-naïve, pachychoroid spectrum disease (CSC/PPE) who had previously undergone thorough clinical assessment and multimodal imaging, including UWF ICGA, EDI-OCT, spectral-domain optical coherence tomography (SD-OCT), fundus photography, fundus autofluorescence (FAF), and UWF fluorescein angiography (FA), as indicated for their ongoing care,

were identified for the study from a vitreoretinal referral practice located in San Ramon, California (JJJ). Prior treatment with laser, photodynamic therapy, and anti-vascular endothelial growth factors was an exclusion criterion; therefore, eyes with PNV and PCV/aneurysmal type 1 neovascularization were not included in this study. Diagnosis of CSC was established based on clinical history, examination, and multimodal imaging identifying the presence or history of exudative retinal detachment with serous PED, characteristic FAF with zones of hyperautofluorescence, geographic speckled hyperautofluorescence, gravitational tracts of hyper- or hypoautofluorescence,⁴³⁻⁴⁵ and EDI-OCT findings of pachychoroid with choroidal thickness >300 µm in any location or an extrafoveal focus exceeding the choroidal thickness of the fovea by at least 50 µm.⁴⁶ FA demonstrated one or multiple focal leaks at the level of RPE, and ICGA showed areas of delayed choroidal filling and prominent venous dilation with leakage.¹³ Diagnosis of PPE was based on clinical history, examination, and multimodal imaging identifying the characteristic reduced fundus tessellation without drusen, mottling of the RPE, and irregular areas of RPE elevation or PEDs.² FAF typically demonstrated mottled hypoautofluorescence and areas of hyperautofluorescence in foci of apparent RPE thickening or hyperplasia.^{13,46} EDI-OCT also demonstrated a thickened choroid and dilated Haller's layer vessels as previously defined by Dansingani et al.⁴⁶ ICGA in PPE eyes typically exhibited leakage and hyperpermeability in the areas of thickened choroid, dilated Haller's vessels, and overlying pigment epitheliopathy.^{13,46} The control, nonpachychoroid patients originally underwent FA and ICGA to evaluate for chorioretinal disease, including suspicious choroidal lesions and tumors and to rule out inflammatory uveitis. Eyes with inflammatory choroiditis were excluded from the control group. Clinical, demographic, and imaging factors were analyzed, including age, gender, eye laterality, visual acuity, central foveal thickness, and subfoveal choroidal thickness.

Ultra-Widefield Indocyanine Green Angiography

Ultra-widefield angiography, including FA and ICGA imaging, was obtained simultaneously after an intravenous injection of an equal mixture of 5 mL 10% sodium fluorescein and 25 mg ICG on the Optos California (P200DTx *icg*; Optos, Inc., Dunfermline, UK), which enabled imaging up to 200 degrees, or 82% of the retina, in a single image. ICGA excitation wavelengths of approximately 800 nm, a cutoff at 807 nm in the barrier filter, and a transmission wavelength extending beyond 900 nm were used. Acquisition of FA and ICGA interweaving images was performed by trained retinal photographers, and the contrast and brightness of each frame were adjusted by the automated algorithm, Auto-Contrast (Optos Advance 4.3; Optos, Inc.) within the Optos California. Images were selected from mid-phases after 2 to 5 minutes from initial dye injection, allowing for complete filling of the choroidal vessels extending to the vortex ampullae without oversaturation of the brightness and late obscuration of the fluorescence signal. Images were reviewed and included based on good centration, minimal eyelid and eyelash artifacts, and view of all four vortex ampullae. Detailed analysis of the patterns of UWF ICGA was correlated with clinical and EDI- and SD-OCT findings.

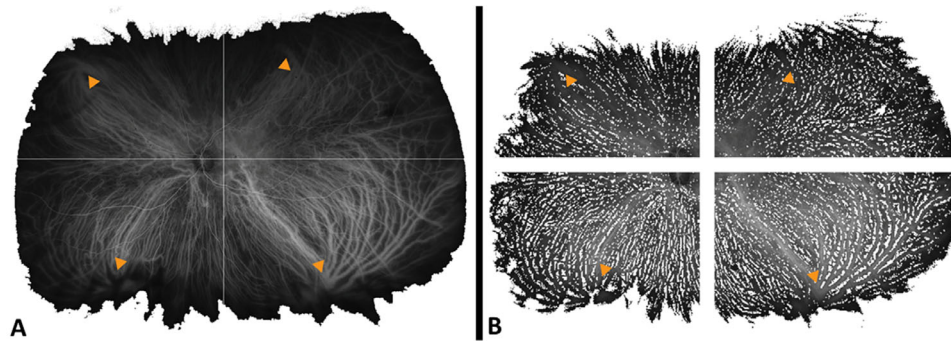


FIGURE 1. Representative mid-phase ultra-widefield indocyanine green angiography images (Optos California; Optos, Inc., Dunfermline, UK) after removal of imaging artifacts from a left eye diagnosed with chronic central serous chorioretinopathy. **(A)** Using multilevel image thresholding with Otsu's method⁴⁷ and local adaptive threshold calculations based on pixel values and **(B)** after segmentation to quadrants based on the most central extension of the choroidal vessel draining into respective vortex veins (yellow arrowheads).

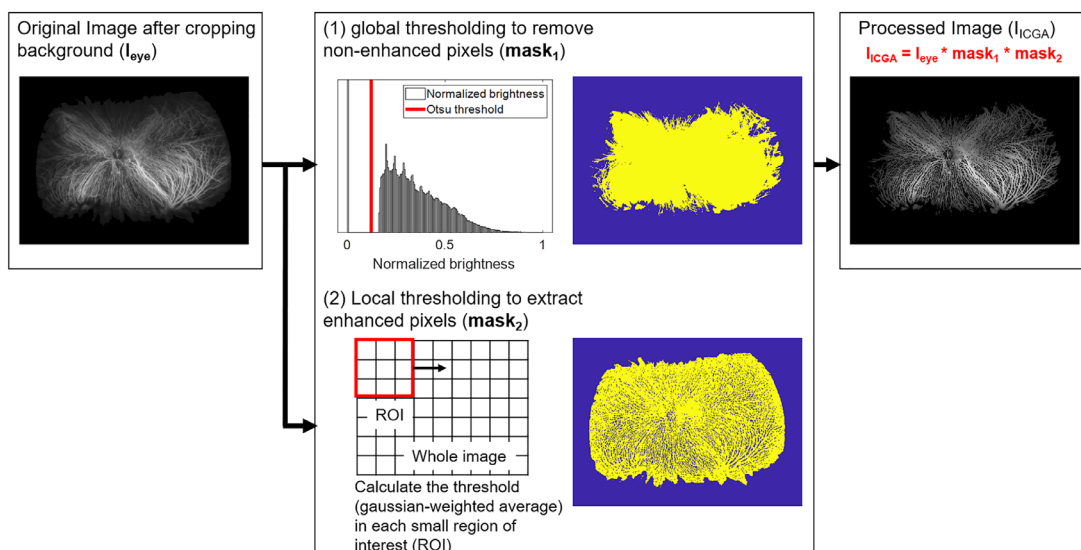


FIGURE 2. Image processing procedure used in this study. Both global and local thresholding methods were employed in parallel for the original image (I_{eye}) for the purpose of removing nonenhanced pixels ($mask_1$) and extracting enhanced pixels ($mask_2$). The final image, which represents the ICGA-enhanced pixels (I_{ICGA}), was the multiplication of I_{eye} , $mask_1$, and $mask_2$.

Image Analysis

Combined FA and ICGA images were processed by cropping the image to remove nonchoroidal imaging artifacts (eyelids and eyelashes) and included only the choroidal vessels and vortex ampullae. All UWF ICGA image size and rotation were standardized. The image was then segmented into quadrants based on the most central extension of the choroidal vessel draining into its respective vortex veins (Fig. 1). Figure 2 describes the detail flow of image processing. The image background was excluded from the segmented image based on pixel values (I_{eye}). Multilevel image thresholding using Otsu's method⁴⁷ was applied to I_{eye} , generating a binarized image and a mask ($mask_1$) of the targeted region for analysis. The pixels with values lower than the predetermined threshold were excluded. Enhanced regions were extracted from I_{eye} using a local adaptive threshold calculated based on the Gaussian weighted average ($mask_2$).⁴⁸ A small region of interest (ROI) was laid over the whole image to compute local-neighborhood threshold. The size of ROI was 3 by

3 pixels, and the foreground was assumed to be brighter than background. The sensitivity factor (that indicated sensitivity toward thresholding more pixels as foreground) was set as 0.63 within the range of [0, 1]. The ICGA-enhanced regions (I_{ICGA}) were extracted by taking the logical sum of I_{eye} , $mask_1$, and $mask_2$. The pixel values, representing intensity described as an 8-bit integer (0 to 255), of the extracted I_{ICGA} were defined as brightness, and the average, standard deviation, and maximum and minimum values were calculated for the entire eye and each quadrant. The number of pixels in I_{eye} and I_{ICGA} was determined, and the ratio of the enhanced region to the entire eye region was calculated. All image processing was performed using MATLAB R2018b with image processing toolbox (MathWorks, Natick, MA).

Statistical Analysis

Within a given eye, the brightness "max-min" value was calculated to assess nonuniformity between four quadrants. Specifically, the quadrant with the least brightness was

TABLE 1. Demographics

Characteristic	Control (<i>n</i> = 16 Eyes of 9 Patients)	Pachychoroid (<i>n</i> = 33 Eyes of 18 Patients)	<i>P</i> Value
Age, y	53.78 ± 17.92	51.94 ± 9.72	0.731
Laterality (right eye)	8 (50.0)	16 (48.5)	0.923
Gender (male)	4 (44.44)	13 (72.22)	0.171
BCVA, logMAR	0.065 ± 0.09	0.169 ± 0.21	0.067
Central foveal thickness (μm)	281.07 ± 16.10	315.91 ± 90.15	0.16
Subfoveal choroidal thickness (μm)	274.50 ± 110.15	477.30 ± 114.23	<0.001

Baseline demographics comparing control eyes to eyes with pachychoroid. Data are presented as mean ± SD or number (%). Bold values denote significance set at $P < 0.05$.

subtracted from the quadrant with the greatest brightness. We plotted the cumulative distribution function to characterize differences in the distribution of max-min brightness value and reported the results from a *t*-test to quantify the mean max-min difference in brightness between pachychoroid eyes and control eyes. A multivariate linear regression was performed to determine, across individual eyes, which specific quadrants had the greatest brightness in pachychoroid eyes, after taking into account patient-eye-specific variability (fixed effects). Specifically, we regressed the average brightness within a quadrant on dummy variables to study each of the quadrants (with the superonasal quadrant, which was the least bright as the reference group) after controlling for patient-eye-specific fixed effects (i.e., including indicator variables for the interaction between patient and eye). Hiroe and Kishi⁴⁹ previously demonstrated that the superonasal vortex vein is the least active in both control and CSC eyes. By using fixed effects for our linear regressions, we accounted for variation in baseline contrast or brightness (along with variation with any other possible confounding variable for which we are unaware) between eyes. Similarly, a multivariate linear regression was performed to determine, across individual eyes, which specific quadrants had the greatest brightness in control eyes. Subsequently, a multivariate linear regression was performed to determine if there were significant differences in brightness within specific quadrants (relative to the first quadrant) across pachychoroid and control eyes. Data was analyzed using the Stata 13.0 statistical package (StataCorp LP, College Station, TX, USA). Significance was set at $P < 0.05$.

RESULTS

Demographics

We included 33 eyes of 18 patients with pachychoroid disease (CSC/PPE) who met the inclusion criteria along with 16 eyes of 9 controls. Within the pachychoroid group, 19 (57.57%) eyes had an active CSC at the time of image acquisition and 14 (42.42%) eyes had PPE. Baseline characteristics are summarized in Table 1 and did not significantly differ between groups aside from subfoveal choroidal thickness. Both pachychoroid and control groups were comparable in terms of age. Average age was 53.78 ± 17.92 years and 51.94 ± 9.72 years for the control and pachychoroid groups, respectively ($P = 0.73$). Fifty percent (8/16) of eyes were right sided in the control group versus 48.5% (16/33) in the pachychoroid group ($P = 0.923$). Gender predominance did not significantly differ between groups, although males composed the majority in the pachychoroid group (13/18, 72.22%) and the minority in the control group (4/9, 44.44%;

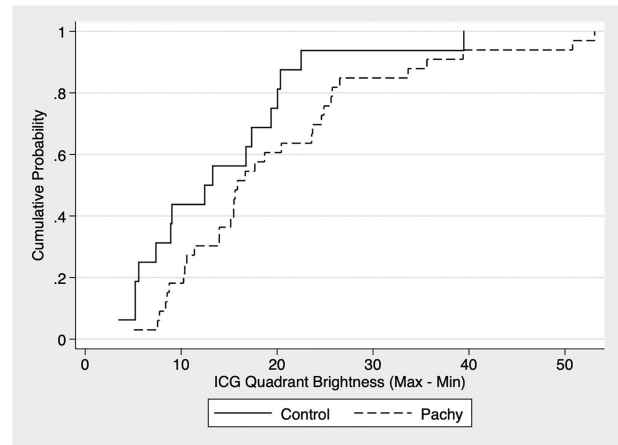


FIGURE 3. Graph of the cumulative distribution function (CDF) of max-min ICGA quadrant brightness. Max-min value of ICGA quadrant brightness is a nonuniformity measure and was calculated by subtracting the brightness level of the quadrant with the least brightness from the quadrant with the greatest brightness in a given eye. Note that pachychoroid eyes (Pachy) uniformly had greater max-min values than control eyes across the board.

$P = 0.171$). Mean logMAR best-corrected visual acuity was comparable between groups at 0.065 ± 0.09 (20/23.75) and 0.168 ± 0.21 (20/33) in the control and pachychoroid groups, respectively ($P = 0.067$). The mean central foveal thickness did not significantly differ between control (281.07 ± 16.10 μm) and pachychoroid eyes (315.91 ± 90.15 μm, $P = 0.16$). Subfoveal choroidal thickness was significantly thicker in the pachychoroid group compared to controls (477.30 ± 114.23 μm vs. 274.50 ± 110.15 μm, $P < 0.001$).

Quantitative UWF ICGA Image Analysis

As described in the Methods section, brightness levels were determined per pixel and averaged within quadrants, with the mean image size per quadrant of 149,493 ± 59,257 pixels (range, 50,613 to 380,497 pixels). The number of pixels (and therefore size of quadrants) did not significantly differ ($P = 0.77$). On average, the max-min brightness within control eyes was 14.15 ± 9.23 units. The average max-min brightness within pachychoroid eyes was 19.85 ± 11.85 units. On average, pachychoroid eyes have max-min brightness that is significantly higher than control eyes (5.66 units, $P < 0.001$).

The cumulative probability density plot (Fig. 3) shows that the cumulative distribution of nonuniform drainage (among vortex veins of a given eye) as measured by max-min brightness for pachychoroid eyes (dashed line) right-shifted

TABLE 2. Multivariate Regression Analysis Comparing Brightness Levels Between Quadrants in Pachychoroid Eyes

Quadrant	Coefficient	Standard Error	t-Statistic	P Value	95% Confidence Interval	
					Lower	Upper
Superonasal	<i>Reference</i>					
Superotemporal	1.04	1.51	0.69	0.493	-1.95	4.02
Inferonasal	9.35	1.51	6.19	<0.001	6.35	12.34
Inferotemporal	17.23	1.98	8.72	<0.001	13.31	21.16

Multivariate linear regression analysis was performed comparing average brightness level between quadrants in pachychoroid eyes, controlling for patient-eye-specific fixed effects (i.e., including indicator variables for the interaction between patient and eye). More positive values correspond to brighter quadrants. Bold values denote significance set at $P < 0.05$.

TABLE 3. Multivariate Regression Analysis Comparing Brightness Levels Between Quadrants in Control Eyes

Quadrant	Coefficient	Standard Error	t-Statistic	P Value	95% Confidence Interval	
					Lower	Upper
Superonasal	<i>Reference</i>					
Superotemporal	0.14	2.29	0.06	0.951	-4.48	4.76
Inferonasal	3.99	2.02	1.98	0.054	-0.08	8.06
Inferotemporal	9.72	2.00	4.87	<0.001	5.70	13.74

Multivariate linear regression analysis was performed comparing average brightness level between quadrants in control eyes without pachychoroid, controlling for patient-eye-specific fixed effects (i.e., including indicator variables for the interaction between patient and eye). More positive values correspond to brighter quadrants. Bold values denote significance set at $P < 0.05$.

relative to that of control eyes (solid line), indicating that pachychoroid eyes have higher max-min brightness relative to control eyes throughout the distribution. This indicates that across the board, pachychoroid eyes were observed to be more prone to having nonuniform drainage in between vortex veins as compared to control eyes.

Multivariate Regression Analysis

Among pachychoroid eyes, the inferonasal and inferotemporal quadrants were both significantly brighter compared to the superonasal quadrant at 9.35 units ($P < 0.001$) and 17.23 units ($P < 0.001$), respectively (Table 2). When evaluating the individual cohorts of CSC and PPE individually, we found similar asymmetrical brightness of the inferonasal (CSC: 11.03 units, $P < 0.001$; PPE: 7.06 units, $P = 0.018$) and inferotemporal quadrants (CSC: 16.36 units, $P < 0.001$; PPE: 18.43, $P < 0.001$) (Supplementary Tables S2A, S2B). We repeated the same exercise for control eyes and found that similar to pachychoroid eyes, both the inferonasal and inferotemporal quadrants were brighter than the

superonasal quadrant, although the magnitudes of the differences were significantly smaller. Specifically, among control eyes, on average, the inferonasal quadrant was marginally brighter than the superonasal quadrant at 3.99 units ($P = 0.054$) while the inferotemporal quadrant was significantly brighter than the superonasal quadrant (9.72 units, $P < 0.001$; Table 3). Overall, after adjusting for the preferential, nonuniform drainage in control eyes, the inferonasal and inferotemporal quadrants in pachychoroid eyes were significantly brighter than the reference quadrant by 5.36 units ($P = 0.034$) and 7.51 units ($P = 0.008$), respectively (Table 4). Similarly, when evaluating the individual cohorts of CSC and PPE separately and adjusting for preferential, nonuniform drainage in control eyes, we observed similar statistically significant asymmetrical brightness of the inferonasal for CSC (7.04 units, $P = 0.006$) but not for PPE (3.07 units, $P = 0.383$) due to a small sample size. The inferotemporal quadrants (CSC: 6.64 units, $P = 0.017$; PPE: 8.71, $P = 0.052$) were significantly different in comparison to the reference group (Supplementary Tables S4A, S4B). These differences in brightness level per quadrant are further illustrated

TABLE 4. Multivariate Regression Analysis Comparing Brightness Levels Between Quadrants in Pachychoroid Eyes Adjusted for Values From Control Eyes

Quadrant	Coefficient	Standard Error	t-Statistic	P Value	95% Confidence Interval	
					Lower	Upper
Superonasal	<i>Reference group</i>					
Superotemporal	0.89	2.73	0.33	0.743	-4.49	6.28
Inferonasal	5.36	2.51	2.14	0.034	0.40	10.31
Inferotemporal	7.51	2.80	2.68	0.008	1.98	13.05

Multivariate linear regression analysis was performed comparing average brightness level between quadrants in pachychoroid eyes, after adjusting for preferential, nonuniform drainage in controls eyes. Patient-eye-specific fixed effects were controlled in the regression (i.e., including indicator variables for the interaction between patient and eye). More positive values correspond to brighter quadrants. Bold values denote significance set at $P < 0.05$.

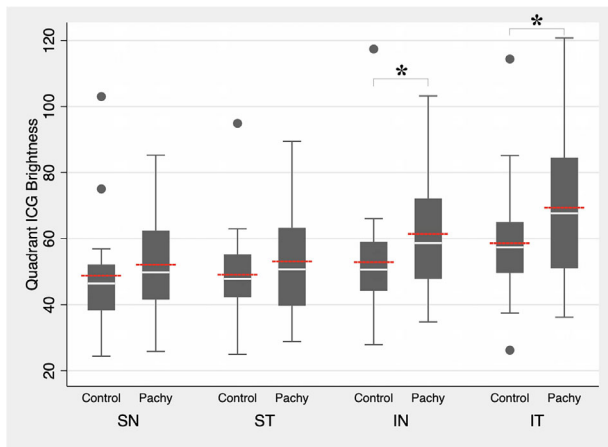


FIGURE 4. Intraquadrant comparison of quadrant brightness level between control and pachychoroid eyes. *White lines* indicate median value. *Red lines* indicate mean value. Boxplots indicate minimum, 25th percentile, 75th percentile, and maximum values. ICG, indocyanine green; IN, inferonasal quadrant; IT, inferotemporal quadrant; Pachy, pachychoroid eyes; SN, superonasal quadrant; ST, superotemporal quadrant. *Significant at $P < 0.05$ comparing mean values.

in Figure 4. Although not significant, since there was a difference in the gender composition between the control and pachychoroid groups, we confirmed that the results were essentially unchanged when analyzing only male subjects.

DISCUSSION

The majority of the clinical manifestations of CSC, PPE, and the pachychoroid spectrum of disease is concentrated within the macular region.^{1,2,8,9,11,13} However, advances in ultra-widefield imaging technology have previously demonstrated extensive peripheral retinal involvement in patients with CSC, beyond that of the field detectable by standard nonwidefield imaging.^{36,38,50} In our study, we used mid-phase images from UWF ICGA and quantitatively compared brightness levels between quadrants of a given eye. This max-min analysis comparing the nonuniformity between four quadrants and subtracting the quadrant with the least brightness from the quadrant with the greatest brightness within a given eye allowed for independent measurement of pixels correlating to brightness across the pachychoroid and control groups. The cumulative probability density (Fig. 3) revealed significant nonuniformity in ICGA dye drainage through vortex veins between quadrants at every percentile in pachychoroid (CSC/PPE) eyes compared to normal controls. When limiting our analysis to only eyes with CSC or only eyes with PPE separately, similar trends were found (Supplementary Tables S2A, S2B, S4A, S4B).

Multimodal imaging of the pachychoroid spectrum has previously demonstrated that the pathology appearing within the macula is due to RPE dysfunction with underlying choroidal thickening, dilation of Haller's layer vessels, and choroidal hyperpermeability on angiography due to attenuation of the overlying choriocapillaris in areas of dilated deep choroidal vessels.^{6,7,13,14,22,29-31} Studies have demonstrated with en face swept-source OCT that pachychoroid eyes have dilated deep choroidal vessels concentrated in areas of maximal choroidal thickness that remain abnormally enlarged in contrast to the physiologic tapering of caliber that normally occurs as vessels approach their most posterior extent.^{46,49}

The origin of the abnormal pachychoroid vessels appeared to extend from outside of the swept-source viewing parameters (a 12×9 -mm area). The authors hypothesized that this may be attributable to systemic factors such as elevated serum cortisol or local factors such as outflow congestion.^{20,22-28,46}

Using UWF ICGA, Pang et al.³⁸ reported based on subjective grading of fluorescence varying degrees of choroidal vessel dilation along the entire drainage course toward individual vortex vein ampullae, suggesting outflow congestion as the cause of the posterior manifestations of CSC.^{20,22-28} Furthermore, this theory is supported by significant differences in mean choroidal vessel density (MCVD) in CSC versus control eyes described by Hirahara et al.⁵⁰ after binarizing the choroid in UWF ICGA images. In the same report, significantly higher MCVD was noted in the posterior pole region and inferiorly, similarly seen in both CSC and control eyes. Interestingly, the overall choroidal density was significantly higher among CSC eyes than controls in the entire area, including the macular region and peripheral areas.⁵⁰ These authors surmised that the increase in MCVD was attributed to dilation of choroidal vessels and variable increases in choroidal vessel diameters rather than increases in overall choroidal vessel count.⁵⁰ Similarly, we found that quantitatively based on brightness metrics, pachychoroid eyes have significantly greater nonuniformity in drainage than nondiseased eyes (5.66 units, $P < 0.001$). More specifically, the cumulative probability density plot (Fig. 3) showed that the cumulative distribution of nonuniform drainage (among vortex veins of a given eye) for pachychoroid eyes had a higher max-min brightness relative to control eyes across the board. This drainage asymmetry in the vortex veins was consistent with that described by Hiroe and Kishi,⁴⁹ wherein asymmetric outflow was noted in all CSC eyes as compared to 38% of normal eyes. This difference between pachychoroid and normal eyes may readily explain the presumed mechanism of increased intraluminal hydrostatic pressure leading to enlarged lumens of deep choroidal vessels^{20,22-28,50} extending from the macula to the vortex vein ampullae and may be a characteristic finding within the pachychoroid spectrum.

Results of the multivariate regression model showed significantly brighter inferior quadrants in both control and pachychoroid eyes, relative to superior quadrants. Using a comparison to the superonasal quadrant, the difference in pachychoroid eyes, after adjusting for the preferential, nonuniform drainage in control eyes, demonstrated that the inferonasal and inferotemporal quadrants in pachychoroid eyes continued to be significantly brighter than the reference quadrant by 5.36 units ($P = 0.034$) and 7.51 units ($P = 0.008$), respectively (Table 4). When limiting our analysis to only eyes with CSC or only eyes with PPE separately, similar trends were found (Supplementary Tables S2A, S2B, S4A, S4B). Similarly, Hirahara et al.⁵⁰ demonstrated that the MCVD with binarization in both control eyes was significantly higher ($P < 0.05$, Bonferroni test) in the macula ($37.01\% \pm 1.44\%$) and inferior ($36.98\% \pm 0.88\%$) areas compared to the superior ($31.37\% \pm 0.97\%$) region and, in CSC eyes, significantly higher ($P < 0.01$, Bonferroni test) in the posterior ($41.04\% \pm 0.82\%$) and inferior ($38.65\% \pm 0.27\%$) areas compared to the superior ($34.02\% \pm 0.97\%$) region. Furthermore, previous studies have reported that asymmetric vortex drainage occurred in 38% to 50% of normal control eyes, of which 53% to 67% had preferential drainage superotemporally and 47% inferotemporally,

but no preferential drainage was noted superonasally.^{49,51} Inherently, the difference in brightness levels per quadrant we found in our study presumably reflects the amount of dye and asymmetry in rates of dye clearance in each quadrant. Gravity may explain preferential flow toward the inferior vortex veins,⁵² but another explanation may be a lower rate of dye clearance inferiorly. Venous blood attempting to flow through inferior vortex veins would face a tighter, more circuitous drainage as it flows beyond the inferior medial and lateral vortex veins through the smaller caliber plexus and eventually drains into the superior ophthalmic vein as compared to the vortex drainage superiorly, which drains directly into the superior ophthalmic vein.⁵³

This may explain the finding of asymmetry in drainage in both control and pachychoroid eyes, but the pathophysiology underlying the increased brightness indicative of delayed outflow through the inferior vortex veins in pachychoroid disease remains unclear.^{2,13,21,38} A recent study in cynomolgus monkeys demonstrated that occluding two vortex veins altered the filling pattern and structures of choroidal vessels and led to delayed choroidal filling on ICGA and increased choroidal thickness in the occluded regions.⁵⁴ Interestingly, occlusion of only one vortex vein had little influence on the structural status of the choroid.⁵⁴ These findings suggest that the compensatory anastomotic mechanism of venous blood drainage may be sufficiently efficient to compensate when only one vortex vein is hindered. Perhaps in diseases (such as those within the pachychoroid spectrum), in which there are multiple inferior vortex veins concurrently affected, there may be resulting venous congestion to a level that overwhelms the normal drainage. This could then lead to dilation within the deep, Haller choroidal vessels and result in overlying choriocapillaris attenuation, RPE dysfunction, and subsequent exudation in the posterior pole.³³ As Cheung et al.¹³ surmised, pachychoroid disease may have a heritable component,^{55–58} in addition to environmental factors, that causes an altered response to steroids manifesting as inferior vortex vein ampulla engorgement and outflow asymmetry.

Similar to severe cases of chronic CSC, idiopathic uveal effusion syndrome presents with exudative retinal and ciliochoroidal detachment, oftentimes associated with nanophthalmos or shorter axial lengths.^{38,59} The suggested pathophysiological mechanism was thought to be either due to vortex vein compression secondary to abnormally thickened sclera, which could resolve with vortex vein decompression,⁶⁰ or due to decreased permeability of the sclera that could improve with sclerectomies and sclerostomies.^{61–66} Hiroe and Kishi⁴⁹ hypothesized that a thickened sclera might narrow the scleral tunnel in which the vortex veins penetrate and exit. These authors observed that CSC does not typically occur in highly myopic eyes with thin sclera,⁴⁹ whereas eyes with shorter axial lengths and uveal effusion syndrome are associated with a thickened sclera.^{49,60,61} Venkatesh et al.⁵⁹ described a case of chronic CSC that improved with partial-thickness scleral resection with mitomycin C, and although the authors did mention that the chronic CSC may resolve spontaneously, the dramatic improvement anatomically and visually was thought to be related to the surgical procedure. Although we do not suggest surgical intervention for cases of pachychoroid disease, these observations may explain the structural mechanism inherent within these eyes that leads to vortex vein engorgement and delayed outflow.

The retrospective nature of the study and the number of subjects contribute to the limitations of this study. Moreover, although not statistically significant ($P = 0.17$), the pachychoroid group had a greater representation of males (13 of 18 subjects, 72.22%) when compared to the control group (4/9, 44.44%), which would be expected given the male predominance of CSC.¹³ When reanalyzing our data, after omitting all female subjects, we confirmed that the results were essentially unchanged (data not shown). In addition, the control group included eyes that were not completely normal, and we included eyes imaged with UWF FA and ICGA for chorioretinal diseases, including suspicious choroidal lesions and tumors, and to rule out inflammatory uveitis. These diagnoses may also have increased choroidal thickness and possible outflow restriction, but no included control eyes had diagnosed uveitic choroiditis. We also did not directly measure the diameter and density of the choroidal vessels but rather assessed the brightness levels in each quadrant with which the vessel diameter and density would be directly correlated. Hirahara et al.⁵⁰ previously demonstrated that vessel density correlated to binarized pixelated ICGA images and also observed that choroidal vessel diameter was not significantly different in comparing eyes with and without CSC. Given these results, we did not repeat these measurements but instead assumed the findings of their study were accurate regarding choroidal vessel density and diameter. Instead, we employed a method by which we quantitatively analyzed UWF ICGA images by comparing the quadrant brightness relative to a reference quadrant within the same eye. Using this unique intraeye max-min brightness image analysis technique, we avoided the potential confounding effects of variation in axial length,⁶⁷ refractive error,⁶⁷ and contrast/brightness signal that could influence the results if comparing across eyes instead of within the same eye. Moreover, in our multivariate regression that made comparisons across eyes, we controlled for patient-eye-specific fixed effects, including indicator variables for the interaction between patient and eye, which would also remove any possible effects from confounding variables that differ across eyes (but remains the same within a given eye).

In this study, we also chose to use only mid-phase UWF ICGA images for analysis (due to the consecutive FA and ICGA acquisition feature on the Optos California), which results in only being able to transit one eye at a time. Moreover, we were unable to analyze any temporal differences between early, mid-phase, or late ICGA frames due to the small number of eyes and limited images to compare in both control and pachychoroid eyes. Replications in larger cohorts with multiple phases of ICGA filling may yield more reproducible results. Last, we acknowledge that the pachychoroid spectrum of disease includes PNV and PCV, in addition to CSC and PPE.¹³ However, no eyes with PNV or PCV were included in this study, since prior treatment with laser, photodynamic therapy, and anti-vascular endothelial growth factors was an exclusion criteria. Therefore, our findings may not be generalizable to the entire pachychoroid spectrum of diseases.

Nevertheless, this study describes a novel methodology in quantifying brightness levels per quadrant of mid-phase UWF ICGA within the same eye to evaluate variations in choroidal outflow. Future studies including correlations with other forms of angiography and Doppler imaging that penetrate beyond the sclera will help validate our results. In summary, we demonstrated variations in choroidal venous

outflow in both normal and pachychoroid eyes by quantifying and comparing brightness levels in each quadrant of UWF ICGA. Increased brightness levels along inferior quadrants in mid-phase ICGA images suggest venous outflow congestion among eyes with central serous chorioretinopathy and pachychoroid pigment epitheliopathy.

Acknowledgments

Supported by an unrestricted grant from Research to Prevent Blindness and K08 Grant (QVH, 1 K08 EY023595, National Eye Institute, National Institutes of Health). The sponsor or funding organization had no role in the design or conduct of this research.

Disclosure: **J.J. Jung**, Carl Zeiss Meditec (C), Alimera Sciences (C), Allergan (C), Google (C); **D.J.G. Yu**, None; **K. Ito**, None; **S. Rofagha**, Carl Zeiss Meditec (F); **S.S. Lee**, Carl Zeiss Meditec (F); **Q.V. Hoang**, None

References

- Wang M, Munch IC, Hasler PW, Prunte C, Larsen M. Central serous chorioretinopathy. *Acta Ophthalmol.* 2008;86:126–145.
- Warrow DJ, Hoang QV, Freund KB. Pachychoroid pigment epitheliopathy. *Retina.* 2013;33:1659–1672.
- Yannuzzi L, Gitter K, Schatz H. *Central serous chorioretinopathy.* In: Yannuzzi L, Gitter K, Schatz H, eds. *The Macula: A Comprehensive Text and Atlas.* Baltimore, MD: Williams & Wilkins; 1979:145–165.
- Carvalho-Recchia CA, Yannuzzi LA, Negrao S, et al. Corticosteroids and central serous chorioretinopathy. *Ophthalmology.* 2002;109:1834–1837.
- Haimovici R, Koh S, Gagnon DR, Lehrfeld T, Wellik S; Central Serous Chorioretinopathy Case-Control Study Group. Risk factors for central serous chorioretinopathy: a case-control study. *Ophthalmology.* 2004;111:244–249.
- Imamura Y, Fujiwara T, Margolis R, Spaide RF. Enhanced depth imaging optical coherence tomography of the choroid in central serous chorioretinopathy. *Retina.* 2009;29:1469–1473.
- Maruko I, Iida T, Sugano Y, Ojima A, Sekiryu T. Subfoveal choroidal thickness in fellow eyes of patients with central serous chorioretinopathy. *Retina.* 2011;31:1603–1608.
- Pang CE, Freund KB. Pachychoroid neovascuopathy. *Retina.* 2015;35:1–9.
- Margolis R, Mukkamala SK, Jampol LM, et al. The expanded spectrum of focal choroidal excavation. *Arch Ophthalmol.* 2011;129:1320–1325.
- Pang CE, Freund KB. Pachychoroid pigment epitheliopathy may masquerade as acute retinal pigment epitheliitis. *Invest Ophthalmol Vis Sci.* 2014;55:5252.
- Balaratnasingam C, Lee WK, Koizumi H, Dansingani K, Inoue M, Freund KB. Polypoidal choroidal vasculopathy: a distinct disease or manifestation of many? *Retina.* 2016;36:1–8.
- Lee WK, Baek J, Dansingani KK, Lee JH, Freund KB. Choroidal morphology in eyes with polypoidal choroidal vasculopathy and normal or subnormal subfoveal choroidal thickness. *Retina.* 2016;36(suppl 1):S73–S82.
- Cheung CMG, Lee WK, Koizumi H, Dansingani K, Lai TYY, Freund KB. Pachychoroid disease. *Eye (Lond).* 2019;33:14–33.
- Piccolino FC, Borgia L, Zinicola E, Zingirian M. Indocyanine green angiographic findings in central serous chorioretinopathy. *Eye (Lond).* 1995;9:324–332.
- Yannuzzi LA, Freund KB, Goldbaum M, et al. Polypoidal choroidal vasculopathy masquerading as central serous chorioretinopathy. *Ophthalmology.* 2000;107:767–777.
- Ahuja RM, Downes SM, Stanga PE, Koh AH, Vingerling JR, Bird AC. Polypoidal choroidal vasculopathy and central serous chorioretinopathy. *Ophthalmology.* 2001;108:1009–1010.
- Sasahara M, Tsujikawa A, Musashi K, et al. Polypoidal choroidal vasculopathy with choroidal vascular hyperpermeability. *Am J Ophthalmol.* 2006;142:601–607.
- Negi A, Marmor MF. The resorption of subretinal fluid after diffuse damage to the retinal pigment epithelium. *Invest Ophthalmol Vis Sci.* 1983;24:1475–1479.
- Negi A, Marmor MF. Experimental serous retinal detachment and focal pigment epithelial damage. *Arch Ophthalmol.* 1984;102:445–449.
- Prunte C, Flammer J. Choroidal capillary and venous congestion in central serous chorioretinopathy. *Am J Ophthalmol.* 1996;121:26–34.
- Kitaya N, Nagaoka T, Hikichi T, et al. Features of abnormal choroidal circulation in central serous chorioretinopathy. *Br J Ophthalmol.* 2003;87:709–712.
- Guyer DR, Yannuzzi LA, Slakter JS, Sorenson JA, Ho A, Orlock D. Digital indocyanine green videoangiography of central serous chorioretinopathy. *Arch Ophthalmol.* 1994;112:1057–1062.
- Scheider A, Nasemann JE, Lund OE. Fluorescein and indocyanine green angiographies of central serous chorioretinopathy by scanning laser ophthalmoscopy. *Am J Ophthalmol.* 1993;115:50–56.
- Menchini U, Virgili G, Lanzetta P, Ferrari E. Indocyanine green angiography in central serous chorioretinopathy: ICG angiography in CSC. *Int Ophthalmol.* 1997;21:57–69.
- Spaide RF, Hall L, Haas A, et al. Indocyanine green videoangiography of older patients with central serous chorioretinopathy. *Retina.* 1996;16:203–213.
- Nishiyama Y, Mori K, Murayama K, Yoneya S. Quantitative analysis of indocyanine green angiographic image in central serous chorioretinopathy. *Jpn J Ophthalmol.* 2001;45:116.
- Shiraki K, Moriwaki M, Matsumoto M, Yanagihara N, Yasunari T, Miki T. Long-term follow-up of severe central serous chorioretinopathy using indocyanine green angiography. *Int Ophthalmol.* 1997;21:245–253.
- Iida T, Kishi S, Hagimura N, Shimizu K. Persistent and bilateral choroidal vascular abnormalities in central serous chorioretinopathy. *Retina.* 1999;19:508–512.
- Ersoz MG, Arf S, Hocaoglu M, Sayman Muslubas I, Karacorlu M. Indocyanine green angiography of pachychoroid pigment epitheliopathy. *Retina.* 2018;38:1668–1674.
- Maruko I, Iida T, Sugano Y, Ojima A, Ogasawara M, Spaide RF. Subfoveal choroidal thickness after treatment of central serous chorioretinopathy. *Ophthalmology.* 2010;117:1792–1799.
- Yang L, Jonas JB, Wei W. Choroidal vessel diameter in central serous chorioretinopathy. *Acta Ophthalmol.* 2013;91:e358–e362.
- Maumenee AE. Macular diseases: clinical manifestations. *Trans Am Acad Ophthalmol Otolaryngol.* 1965;69:605–613.
- Gass JD. Pathogenesis of disciform detachment of the neuroepithelium. *Am J Ophthalmol.* 1967;63(suppl):1–139.
- van Velthoven ME, Verbraak FD, Garcia PM, Schlingemann RO, Rosen RB, de Smet MD. Evaluation of central serous retinopathy with en face optical coherence tomography. *Br J Ophthalmol.* 2005;89:1483–1488.
- Verma A, Maram J, Alagorie AR, et al. Distribution and location of vortex vein ampullae in healthy human eyes as assessed by ultra-widefield indocyanine green angiography. *Ophthalmol Retina.* 2020;4:530–534.

36. Klufas MA, Yannuzzi NA, Pang CE, et al. Feasibility and clinical utility of ultra-widefield indocyanine green angiography. *Retina*. 2015;35:508–520.
37. Moriyama M, Cao K, Ogata S, Ohno-Matsui K. Detection of posterior vortex veins in eyes with pathologic myopia by ultra-widefield indocyanine green angiography. *Br J Ophthalmol*. 2017;101:1179–1184.
38. Pang CE, Shah VP, Sarraf D, Freund KB. Ultra-widefield imaging with autofluorescence and indocyanine green angiography in central serous chorioretinopathy. *Am J Ophthalmol*. 2014;158:362–371.e362.
39. Mori H, Yamada H, Sato Y, Takahashi K. Optical coherence tomographic angiography and ultra-widefield indocyanine green angiography of a choroidal macrovessel. *Am J Ophthalmol Case Rep*. 2020;18:100612.
40. Tang PH, Lee MS, van Kuijk FJ. Ultra wide-field indocyanine green angiogram highlights choroidal perfusion delay secondary to giant cell arteritis. *Ophthalmic Surg Lasers Imaging Retina*. 2016;47:471–473.
41. Mackenzie PJ, Russell M, Ma PE, Isbister CM, Maberley DA. Sensitivity and specificity of the Optos Optomap for detecting peripheral retinal lesions. *Retina*. 2007;27:1119–1124.
42. Wessel MM, Nair N, Aaker GD, Ehrlich JR, D'Amico DJ, Kiss S. Peripheral retinal ischaemia, as evaluated by ultra-widefield fluorescein angiography, is associated with diabetic macular oedema. *Br J Ophthalmol*. 2012;96:694–698.
43. Mrejen S, Balaratnasingam C, Kaden TR, et al. Long-term visual outcomes and causes of vision loss in chronic central serous chorioretinopathy. *Ophthalmology*. 2019;126:576–588.
44. Han J, Cho NS, Kim K, et al. Fundus autofluorescence patterns in central serous chorioretinopathy. *Retina*. 2020;40:1387–1394.
45. von Ruckmann A, Fitzke FW, Fan J, Halfyard A, Bird AC. Abnormalities of fundus autofluorescence in central serous retinopathy. *Am J Ophthalmol*. 2002;133:780–786.
46. Dansingani KK, Balaratnasingam C, Naysan J, Freund KB. En face imaging of pachychoroid spectrum disorders with swept-source optical coherence tomography. *Retina*. 2016;36:499–516.
47. Otsu N. A threshold selection method from gray-level histograms. *IEEE Trans Sys Man Cyber*. 1979;9:62–66.
48. Wren CR, Azarbayejani A, Darrell T, Pentland AP. Pfinder: real-time tracking of the human body. *IEEE Trans Pattern Anal Mach Intell*. 1997;19:780–785.
49. Hiroe T, Kishi S. Dilatation of asymmetric vortex vein in central serous chorioretinopathy. *Ophthalmol Retina*. 2018;2:152–161.
50. Hirahara S, Yasukawa T, Kominami A, Nozaki M, Ogura Y. Densitometry of choroidal vessels in eyes with and without central serous chorioretinopathy by wide-field indocyanine green angiography. *Am J Ophthalmol*. 2016;166:103–111.
51. Mori K, Gehlbach PL, Yoneya S, Shimizu K. Asymmetry of choroidal venous vascular patterns in the human eye. *Ophthalmology*. 2004;111:507–512.
52. Shinjima A, Iwasaki K, Aoki K, Ogawa Y, Yanagida R, Yuzawa M. Subfoveal choroidal thickness and foveal retinal thickness during head-down tilt. *Aviat Space Environ Med*. 2012;83:388–393.
53. Cheung N, McNab AA. Venous anatomy of the orbit. *Invest Ophthalmol Vis Sci*. 2003;44:988–995.
54. Chen LL, Wang Q, Yu WH, Chen YX. Choroid changes in vortex vein-occluded monkeys. *Int J Ophthalmol*. 2018;11:1588–1593.
55. Sardell RJ, Nittala MG, Adams LD, et al. Heritability of choroidal thickness in the Amish. *Ophthalmology*. 2016;123:2537–2544.
56. Oosterhuis JA. Familial central serous retinopathy. *Graefes Arch Clin Exp Ophthalmol*. 1996;234:337–341.
57. Miki A, Kondo N, Yanagisawa S, Bessho H, Honda S, Negi A. Common variants in the complement factor H gene confer genetic susceptibility to central serous chorioretinopathy. *Ophthalmology*. 2014;121:1067–1072.
58. de Jong EK, Breukink MB, Schellevis RL, et al. Chronic central serous chorioretinopathy is associated with genetic variants implicated in age-related macular degeneration. *Ophthalmology*. 2015;122:562–570.
59. Venkatesh P, Chawla R, Tripathy K, Singh HI, Bypareddy R. Scleral resection in chronic central serous chorioretinopathy complicated by exudative retinal detachment. *Eye Vis (Lond)*. 2016;3:23.
60. Brockhurst RJ. Vortex vein decompression for nanophthalmic uveal effusion. *Arch Ophthalmol*. 1980;98:1987–1990.
61. Gass JD. Uveal effusion syndrome: a new hypothesis concerning pathogenesis and technique of surgical treatment. *Trans Am Ophthalmol Soc*. 1983;81:246–260.
62. Elagouz M, Stanescu-Segall D, Jackson TL. Uveal effusion syndrome. *Surv Ophthalmol*. 2010;55:134–145.
63. Forrester JV, Lee WR, Kerr PR, Dua HS. The uveal effusion syndrome and trans-scleral flow. *Eye (Lond)*. 1990;4:354–365.
64. Johnson MW, Gass JD. Surgical management of the idiopathic uveal effusion syndrome. *Ophthalmology*. 1990;97:778–785.
65. Faulborn J, Kolli H. Sclerotomy in uveal effusion syndrome. *Retina*. 1999;19:504–507.
66. Uyama M, Takahashi K, Kozaki J, et al. Uveal effusion syndrome: clinical features, surgical treatment, histologic examination of the sclera, and pathophysiology. *Ophthalmology*. 2000;107:441–449.
67. Liu B, Wang Y, Li T, et al. Correlation of subfoveal choroidal thickness with axial length, refractive error, and age in adult highly myopic eyes. *BMC Ophthalmol*. 2018;18:127.